VIII International Conference on Fracture Mechanics of Concrete and Concrete Structures
FraMCoS-8
J.G.M. Van Mier, G. Ruiz, C. Andrade, R.C. Yu and X.X. Zhang (Eds)

MODELLING OF CRACK DEVELOPMENT IN YOUNG CONCRETE

JAN CERVENKA[*], LIBOR JENDELE[*] AND VIT SMILAUER[†]

[*] Cervenka Consulting s.r.o
Na Hrebenkach 2667/55, 150 00, Praha 5, Czech Republic
e-mail: jan.cervenka@cervenka.cz, www.cervenka.cz

[†] Czech Technical University, Prague (CTU)
Thakurova 7, 160 00, Praha 5, Czech Republic
e-mail: smilauer@post.cz, www.fsv.cvut.cz

Key words: hydro-thermo-mechanical analysis, hydration, multi-scale model, affinity model

Abstract: A suitable control of cracking of young concrete often determines the durability and the reliability of concrete structures. A hydro-thermo-mechanical approach is presented for analysis of reinforced concrete structures applicable in engineering practice. The multi-physics problem is solved by a staggered analysis that consists of two steps. The moisture and heat transport analysis is performed and the results are time dependent moisture and temperature fields in all material points. These resulting fields are then used in a stress analysis to calculate stresses, crack patterns and crack width. The whole model is implemented in a finite element software [1], which is used in the validation as well as in a practical application example.

1 INTRODUCTION

The cracking of concrete in early-age due to hydration heat or concrete shrinkage can significantly reduce the durability [2]. In order to prevent early-age cracking, various precautions have been already proposed and implemented into guidelines and codes [3]. The situation complicates in the cases of modern unique structures with insufficient previous experience. In such cases, computer simulation and modelling can help engineers to develop an suitable material design in terms of concrete composition, curing, insulation, cooling etc. In this paper coupled approach is described for hydro-thermo-mechanical analysis of hydrating concrete structures. The model takes into account hydration heat, concrete composition, reinforcement, shrinkage and creep.

A large number of models have been published to account for hydration heat with a transition to creep and shrinkage of reinforced concrete structures [4], [5], [6], [7] . As creep and shrinkage depends strongly on moisture and temperature, heat and moisture transport analyses are essential parts of the mechanical creep analyses. Heat/moisture transport analysis was presented and validated in a previous paper [8]. Here, the extension to mechanical part is proposed and validated.

The hydro-thermo-mechanical model implemented in ATENA software [1] is now suited for material and structural engineers. A sensitive concrete composition with its individual constituents is treated in detail. The reason lies in a variety of concrete composition concerning cement content, aggregate type, fillers, all of them having effects on released heat during hydration, thermal conductivity and capacity.

The developed model is validated using the results of the international benchmark for control of cracking in R/C structures taking place in the year 2010 and known as the ConCrack. The presented model was also

applied to practical engineering problem that appeared during the construction of massive columns (5x5x4.57m) in a new power plant.

2 HEAT AND MOISTURE TRANSPORT ANALYSIS

In young concrete, heat and moisture transport analysis plays an essential influencing the cracking and shrinkage. Fourier law is used to calculate heat transport in the structure. The corresponding governing equation reads

$$\frac{\partial}{\partial t}(Q) = -div(\underline{q}_T) \tag{1}$$

where Q is the total amount of heat accumulated in a unit volume, [J/m^3]. Q can be decomposed to

$$\begin{aligned} Q &= Q_0 + \int \frac{\partial Q}{\partial T} dT + Q_h \\ \frac{\partial Q}{\partial t} &= \frac{\partial Q}{\partial T}\frac{\partial T}{\partial t} + \frac{Q_h}{\partial t} = C_T \frac{\partial T}{\partial t} + \frac{\partial Q_h}{\partial t} \end{aligned} \tag{2}$$

where C_T is heat capacity [J/(K.m^3)], Q_h is total hydration heat at time t, [J/m^3] and $\underline{q}_T$ is heat flux [J/(s.m^2)]. Heat flux $\underline{q}_T$ is calculated using

$$\underline{q}_T = -\mathbf{\Lambda}\underline{\nabla}(T) \tag{3}$$

$\mathbf{\Lambda}$ stands for tensor of heat conductivities, e.g. [J/(s.m.K)] and T is temperature, [^{0}C].

The analysis is based on the calibrated affinity hydration model [8]. It accounts for all stages of cement hydration and calculates the rate of degree of hydration α, $\alpha \in \langle 0...1 \rangle$ The model utilizes chemical affinity $\tilde{A} = \tilde{A}(\alpha)$, [s^{-1}], which is determined for an isothermal temperature 25^{o}C

$$\frac{\partial \alpha}{\partial t} = \tilde{A}_{25} \exp\left[\frac{E_a}{R}\left(\frac{1}{T_{25}} - \frac{1}{T}\right)\right] \tag{4}$$

where R is gas constant $8314.41 \frac{\text{J}}{\text{kmol K}}$, T is current temperature [K], T_{25} is a reference temperature [K], and the activation energy E_a is approximately 40 kJ/mol. Having history of α, the hydration heat released from a unit cement is calculated as:

$$\frac{Q_h}{Q_{h,pot}} \approx \alpha \tag{5}$$

$$\frac{1}{Q_{h,pot}}\frac{\partial Q_h}{\partial t} = \frac{\partial \alpha}{\partial t} = \tilde{A}_{25} \exp\left[\frac{E_a}{R}\left(\frac{1}{T_{25}} - \frac{1}{T}\right)\right] \tag{6}$$

where $Q_{h,pot}$ is potential hydration heat, [J/kg]. Concrete is treated as a five-component medium, composed from cement, water, aggregates, filler and air. Scaling of hydration heat to the concrete occurs from a known composition. Each component carries information about its capacity and conductivity.

Heat capacity of concrete is computed by proportional summation of the present constituents in the concrete mixture. The components' contribution coefficients are their volumetric fractions, i.e. $f_{aggregate}$, f_{filler} and $f_{paste} = f_{water} + f_{cement}$.

$$C_{concrete} = f_{aggregate}C_{aggregate} + f_{filler}C_{filler} + \hat{C}_{paste} \tag{7}$$

where $C_{concrete}$, $C_{aggregate}$, C_{filler} and $\hat{C}_{paste}$ stand for concrete, aggregate, filler and paste capacity (per unit volume). The last term, C_{paste}, depends also on the degree of hydration α and is calculated by

$$\begin{aligned} \hat{C}_{paste} = &\left(f_{cement}C_{cement} + f_{water}C_{water}\right) \\ &\times\left(1 - 0.26\left(1 - e^{-2.9\alpha}\right)\right) \end{aligned} \tag{8}$$

where C_{cement} is cement capacity at time zero [9].

The thermal conductivity of concrete is calculated via homogenization principles. Consider conductivity of cement paste λ_{paste} and aggregates $\lambda_{aggregate}$ such that $\lambda_{paste} \le \lambda_{aggregate}$. The corresponding volume fractions are $f_{paste}, f_{aggregate}$. The Hashin-

Shtrikman lower $\lambda_{concrete,low}$ and upper bounds $\lambda_{concrete,upper}$ [9] reads

$$\lambda_{concrete,low,\infty} = \lambda_{paste} + \frac{3 f_{aggregate} \lambda_{paste} \left(\lambda_{aggregate} - \lambda_{paste}\right)}{3\lambda_{paste} + f_{paste} \left(\lambda_{aggregate} - \lambda_{paste}\right)}$$
$$\lambda_{concrete,upper,\infty} = \lambda_{aggregate} + \frac{3 f_{paste} \lambda_{aggregate} \left(\lambda_{paste} - \lambda_{aggregate}\right)}{3\lambda_{aggregate} + f_{aggregate} \left(\lambda_{paste} - \lambda_{aggregate}\right)} \quad (9)$$

The chain approach delivers conductivities at four scales in the following order:

1. Homogenize phases cement and water to obtain cement paste. Use average of $\lambda_{low,\infty}, \lambda_{upper,\infty}$ [9].
2. Homogenize cement paste and filler. Use average of $\lambda_{low,\infty}, \lambda_{upper,\infty}$.
3. Homogenize the latter with air. Use maximum of $\lambda_{low,\infty}, \lambda_{upper,\infty}$, which corresponds to Mori-Tanaka scheme with air as an inclusion.
4. Homogenize the latter with aggregates to arrive on concrete scale. Use average of $\lambda_{low,\infty}, \lambda_{upper,\infty}$.

The concrete conductivity at time t is calculated as:

$$\lambda_{concrete} = \lambda_{concrete,0} \left(1.0 - 0.248\alpha\right) \quad (10)$$

where $\lambda_{concrete,0}$ is the conductivity of fresh concrete obtained from the four-step homogenization.

The presented model makes no difference between water and water vapour in terms of mass. The governing equations for transport per unit volume reads

$$\frac{\partial w}{\partial t} + \frac{\partial w_h}{\partial t} = -div(\underline{q}_h)$$
$$C_h \frac{\partial h}{\partial t} + \frac{\partial w_h}{\partial t} = -div(\underline{q}_h) \quad (11)$$

where w is moisture content at current time t, [kg/m^3], w_h stands for the amounts of moisture consumed by hydration, [kg/m^3], $\underline{q}_h$ is moisture flux, [kg / (m^2 s)]. t represents time, [s] and h relative humidity. The moisture flux is computed by

$$\underline{q}_h = -\mathbf{D}_h \nabla h \quad (12)$$

where ∇h is a gradient of relative humidity.

Experiments show that 1 kg of cement consumes approximately about 0.23 kg of water when hydrating completely, i.e. typically $Q_{w,pot}$=0.23 kg/kg Assuming a linear dependence between water consumption w^h and degree of cement hydration, the water sink term yields:

$$C_{h,t} = \frac{\partial w_h}{\partial t} = \frac{\partial w_h}{\partial \alpha} \frac{\partial \alpha}{\partial t} \quad (13)$$
$$w_h = Q_{w,pot} c \alpha \quad (14)$$

where c stands for the mass of cement in 1m^3 of concrete

A simple constitutive law based on Kuenzel [10] is used to calculate moisture capacity of concrete, see Equation (15). It has two material constants, namely the free water saturation w_f,[kgm^{-3}], and a dimensionless approximation factor b. The Moisture content in a unit volume w,[kgm^{-3}], is:

$$w = w_f \frac{(b-1)h}{b-h} \quad (15)$$

The parameter b can be determined from the water content w_{80} at relative humidity $h = 0.8$

$$b = \frac{h(w_f - w_{80})}{w_f h - w_{80}} \quad (16)$$

The moisture capacity C,$\left[\text{kgm}^{-3}\right]$ is calculated as a derivative of moisture content with respect to h

$$C_h = \frac{\partial w}{\partial h} = \frac{w_f (b-1) b}{(b-h)^2} \quad (17)$$

Although the model is fairly simple, it provides reasonable accuracy.

3 MECHANICAL ANALYSIS

The mechanical analysis represent the next step in the staggered hydro-thermal solution. The quasi-static formulation accounts for time related phenomena such as creep and shrinkage in hardening concrete. The presented model is suitable for solution of

reinforced concrete structures with large displacements and large rotations.

The crucial feature of the developed model is to separate short-term and long-term material behaviour. The short-term model captures material response, such as concrete fracture, while the long-term model delivers concrete creep. The parameters for the short-time model are changing in time, which is controlled by the long-term material model.

The results from the heat/moisture analysis and mechanical analysis are interpolated to the integration points of the stress analysis by isoparametric interpolation in order to enable the usage of different meshes in both problems.

3.1 Long-term material model

Time effects on concrete behaviour in the long-term material model are incorporated via Stieltjes integral [11],

$$\varepsilon(t) = \int_{t'}^{t} \Phi(t,t')d\sigma + \varepsilon^0(t), \tag{18}$$

where $\sigma(t)$ = stress in time t, $d\sigma$ = stress increment, $\varepsilon^0(t)$ = material swelling/shrinkage at time t, (it accounts for shrinkage/expansion due to temperature change and autogenous shrinkage), $\Phi(t,t')$ = compliance function of concrete creep, t = time at observation and t' = time at loading.

The assumption of linear creep limits the use to cases, where (in long-term time span) structural compression stresses do not exceed about 60% of the concrete strength in compression. However, as creep analysis is typically carried out for structural serviceability conditions, this limitation typically does not pose a problem. Equation (18) is integrated (in time) by Step-by-step method (SBS), in which original material compliance function is replaced by Dirichlet series [12, 13]. Having known stress and strain at the beginning of the time step Δt, i.e. at time t, the values at the end the step. i.e. at time $t+\Delta t$ are calculated as follows, see [13],

$$\Delta\sigma_t = \hat{\mathbf{E}}_t \left(\Delta\bar{\varepsilon}_t - \Delta\hat{\bar{\varepsilon}}_t \right) \tag{19}$$

$$\bar{\varepsilon}_{t+\Delta t} = \bar{\varepsilon}_t + \Delta\bar{\varepsilon}_t \tag{20}$$

$$\bar{\sigma}_{t+\Delta t} = \bar{\sigma}_t + \Delta\bar{\sigma}_t \tag{21}$$

where $\Delta\bar{\sigma}_{t+\Delta t}$ and $\bar{\varepsilon}_{t+\Delta t}$ are the total stress and the total strain at the time $t+\Delta t$. $\hat{\mathbf{E}}_t$ is time adjusted material rigidity matrix and $\Delta\hat{\bar{\varepsilon}}_t$ is vector of artificial strains to simulate the effect of creep in the material. In this work the B3 creep model was used [14].

Creep and shrinkage behaviour of concrete depends on current humidity and temperature conditions. Therefore the results of moisture and humidity analysis can be used to calculate temperature and humidity histories (at each material point of the structure). The effect of the variable temperature $T(t)$ is projected to the creep prediction model by using so-called equivalent time values $t_e(T,t)$. If the creep prediction material law is calibrated for constant reference temperature T_{ref}, then for the varying temperature conditions $T(t)$, the accurate results are obtained by replacement of all real times t by the equivalent times t_e [14].

Each structural material point has its distinct temperature history and hence distinct creep prediction material parameters. However, as the differences between temperature histories (and thus in calculation t_e) of neighbouring material points are often small, it suffices to use only a couple of "master" or "average" temperature histories. The original material point history is then replaced by the closest master history. This approach significantly reduces number of required material parameters sets.

3.1 Short-term material model

The short-term material model accounts for all nonlinear behaviour due to crack developments, material hardening and softening etc. Its prediction heavily depends on current stress-strain conditions in each material point and possibly also on its history. The variable parameters, mainly Young's modulus, initial strains, compressive and tensile strengths etc. are at a particular time

computed by the linear creep model described above.

The short-term concrete mechanical model follows the original theory in [15]. The material model formulation is based on the strain decomposition into elastic ε_{ij}^{e}, plastic ε_{ij}^{p} and fracturing ε_{ij}^{f} components [16].

$$\varepsilon_{ij} = \varepsilon_{ij}^{e} + \varepsilon_{ij}^{p} + \varepsilon_{ij}^{f} \tag{22}$$

The new stress state is then computed by the formula:

$$\sigma_{ij}^{n} = \sigma_{ij}^{n-1} + E_{ijkl}(\Delta\varepsilon_{kl} - \Delta\varepsilon_{kl}^{p} - \Delta\varepsilon_{kl}^{f}) \tag{23}$$

Tensile behaviour of concrete is modelled by non-linear fracture mechanics with a simple Rankine-based criterion.

$$F_i^{f} = \sigma_i'^{t} - f_{ti}'(w_i') \le 0 \tag{24}$$

A smeared crack concept is adopted with the following parameters: tensile strength f_t, shape of the stress-crack opening curve $f_t(w)$ and fracture energy G_F. It is assumed that strains and stresses are converted into the material directions, which in a case of rotated crack model correspond to the principal stress directions, and in a case of a fixed crack model to the principal directions at the onset of cracking. Therefore, $\sigma_i'^{t}$ identifies the trial stress and f_{ti}' tensile strength in the material direction i. The prime symbol denotes quantities in the material directions. This approach is combined with the crack band method of Bažant and Oh [17]. In this formulation, the cracking strain is related to the element size. Consequently, the softening law in terms of strains for the smeared model is calculated for each element individually, while the crack-opening law is preserved. The model uses an exponential softening law of Hordijk [18].

The compressive behaviour is modelled using a plasticity-based model with failure surface defined by the three-parameter criterion form [19]

$$F_{3P}^{p} = \left[\sqrt{1.5}\frac{\rho}{f_c}\right]^2 + m\left[\frac{\rho}{\sqrt{6}f_c}r(\theta,e) + \frac{\xi}{\sqrt{3}f_c}\right] - c = 0 \tag{25}$$

where

$$m = 3\frac{f_c^2 - f_t^2}{f_c\, f_t}\frac{e}{e+1}$$

$$r(\theta,e) = \frac{4(1-e^2)\cos^2\theta + (2e-1)^2}{2(1-e^2)\cos\theta + (2e-1)\left[4(1-e^2)\cos^2\theta + 5e^2 - 4e\right]^{\frac{1}{2}}} \tag{26}$$

In the above equations, (ξ,ρ,θ) are Heigh-Vestergaard coordinates, and f_c and f_t are compressive strength and tensile strength respectively. Parameter $e \in \langle 0.5, 1.0\rangle$ defines the roundness of the failure surface.

The surface evolves during the yielding/crushing process by the hardening/softening laws based on equivalent plastic strain defined as

$$\Delta\varepsilon_{eq}^{p} = \min(\Delta\varepsilon_{i}^{p}) \tag{27}$$

Hardening $\varepsilon_{eq}^{p} \in \langle -\varepsilon_c^{p}; 0\rangle$:

$$f_c(\varepsilon_{eq}^{p}) = f_{co} + (f_c - f_{co})\sqrt{1 - \left(\frac{\varepsilon_c^{p} - \varepsilon_{eq}^{p}}{\varepsilon_c^{p}}\right)^2} \tag{28}$$

Softening $\varepsilon_{eq}^{p} \in \langle -\infty; -\varepsilon_c^{p}\rangle$:

$$\begin{aligned} &c = \left(1 - \frac{w_c}{w_d}\right)^2, \quad w_c \in \langle -w_d; 0\rangle \\ &c = 0, \quad w_c \in (-\infty; w_d) \\ &w_c = (\varepsilon_{eq}^{p} - \varepsilon_c^{p})\, L_c \end{aligned} \tag{29}$$

When concrete crushing enters into the softening regime, an analogous approach to the crack band model is used also for the localization in compression within the crushing band L_c. A direct return-mapping algorithm is used to solve the predictor-corrector equation of the plasticity model.

$$F^{p}(\sigma_{ij}^{t} - \sigma_{ij}^{p}) = F^{p}(\sigma_{ij}^{t} - \Delta\lambda l_{ij}) = 0 \tag{30}$$

The plastic stress σ_{ij}^{p} is a product of plastic multiplier $\Delta\lambda$ and the return direction l_{ij}, which is defined as follows

$$l_{ij} = E_{ijkl}\frac{\partial G^{p}\left(\sigma_{kl}^{t}\right)}{\partial \sigma_{kl}} \tag{31}$$

$$\Delta\varepsilon_{ij}^{p} = \Delta\lambda\frac{\partial G^{p}(\sigma_{ij}^{t})}{\partial \sigma_{ij}} \tag{32}$$

The plastic potential G^{p} is given by

$$G^{p}(\sigma_{ij}) = \beta\frac{1}{\sqrt{3}}I_1 + \sqrt{2J_2} \tag{33}$$

where β determines the return direction. If $\beta < 0$, material is being compacted during crushing, if $\beta = 0$, the material volume is preserved, and if $\beta > 0$, the material is dilating.

A special iterative algorithm [15] analogous to multi-surface plasticity is used to solve the plastic and fracture models such that the final stress tensors in both models are identical.

The presented model is aimed to calculate primarily reinforced concrete structures. In such particular case, two material laws are used; the above described model for adjacent concrete and a 1D model for reinforcement. The latter model can be any time-independent model, such a multi-linear 1D model, or elasto-plastic model with hardening etc.

4 VALIDATION

A validation of the presented model shown using the example from ConCrack benchmark experiment RG8. For further information see http://www.concrack.org/. Figure 1 shows the overall geometry of the beam RG8 with two massive heads on both sides and two restraining steel struts. The central beam part has dimensions 0.5x0.8x5.1 m and is reinforced. The benchmark experiment provides data on cement mineral composition, cement fineness, concrete composition, reinforcement, geometry, external temperature, internal temperature in three points, adiabatic concrete temperature and displacements of two points C,D located on the beam axis 2.5 m apart.

In the first step, the adiabatic experiment was used to validate the hydration model. The model predicts correctly the temperature rise by calibrating only the length of the dormant period. Based on these results the four-parametric affinity model was calibrated [8]. Parameters of the affinity model are B_1=1.8 h^{-1}, B_2=1.0e-5, η=7.0, DoH_∞ = 0.90. Figure 4 demonstrates that both models approximated reasonably well experimental data, especially at younger ages. It reveals clear negative slope documenting the energy loss in the adiabatic experiment.

Figure 1: A validated massive beam RG8 with restrained shrinkage (image and data from the database Cheops).

The same numerical model was used for the heat/moisture transport and mechanical analysis (see Figure 3). Note that the head sizes were reduced and the struts are directly next to the central beam surfaces.

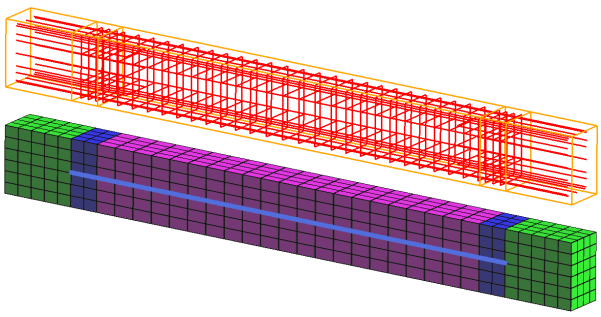

Figure 2: Our model showing the reinforcement and material assignment.

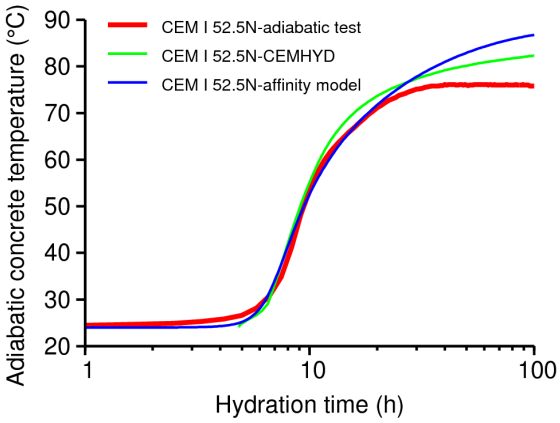

Figure 3: Validation of CEMHYD3D model and the affinity model in concrete adiabatic test.

The pilot calculation revealed that clinker content in the cement CEM I had to be lower than declared. The middle beam was thermally insulated by a layer of 200 mm of expanded polystyrene since the casting. From the chemical composition, the potential energy of the clinker is 498 J/g of cement. The original concrete composition stated 400 kg/m^3 of cement, which would lead to temperatures exceeding 70^{o}C as in the adiabatic experiment. In reality, maximum measured temperature was only 53.7^{o}C at 30 hours of hydration. For this reason, it was decided to reduce the cement content to 320 kg/m^3. Figure 5 shows the temperatures in the bottom sensor located 50 mm above the surface and in the core of the beam. After two days of hydration the expanded polystyrene was stripped off and the beam surface was exposed to ambient air temperature. The experimental temperatures are a bit higher, probably due to additional supply of solar energy, which was not considered in the model. After approximately 4 days, the beam temperatures follow the ambient air fluctuations. The relative humidity drops to 0.88 uniformly in the cross section.

The mechanical analysis assumes standard parameters of ATENA concrete C50/60. Five concrete parameters evolve with time. They are listed in the following table including their values at 28 days.

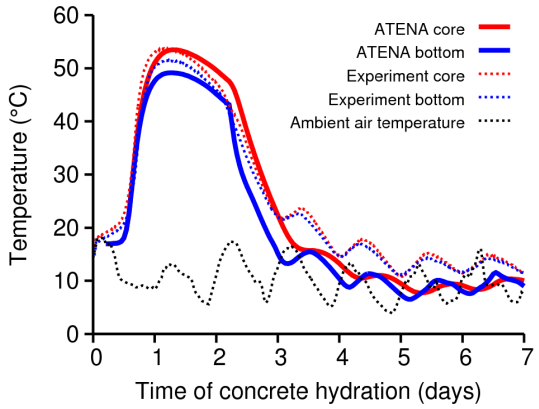

Figure 4: Validation of core and bottom temperature.

Table 1: Mechanical time adjusted parameters for concrete C50/60, w/c=0.475.

Mechanical parameter at 28 days	**Value**
Cylindrical compressive strength	50 MPa
Young's modulus	37 GPa
Compressive stress at the onset of cracking	4.1 MPa
Tensile strength	1.93 MPa
Fracture energy	48.3 J/m^2

The autogeneous shrinkage was calibrated from the measured data and does not play a significant role in this concrete with w/c=0.475. The actual humidity is passed to drying shrinkage function which follows the evolution given by B3 model [14].

For the sake of simplicity our model did not consider wings to which the struts are attached, see Figure 3. This was done in order to avoid complexity with additional reinforcement and transverse pre-stressed tendons in the heads. Therefore, the bracing effect of the struts and wings is maintained by reducing the cross-section area of the struts to 25%. Figure 6 demonstrates the effect of strut bracing. The measure points C,D are 2.5 m apart located on the beam axis. The stiffness reduction has effect up to 3 days of hydration. Afterwards, the displacement of points C,D is controlled by fluctuating temperature of ambient air, straining the struts.

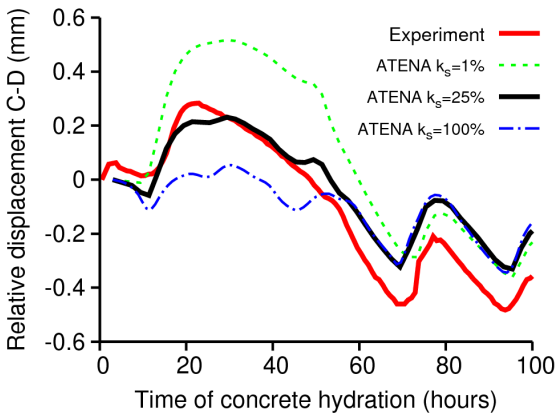

Figure 5: Validation of relative displacements of points C-D with mutual distance 2.5 m on the beam axis. The coefficient k_s shows stiffness reduction of the struts.

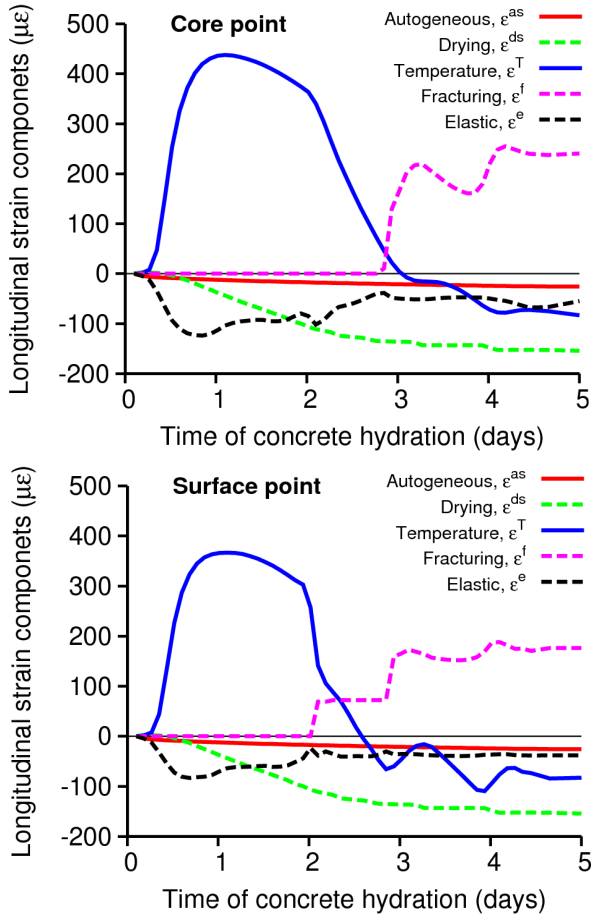

Figure 6: Strain components in the core and surface point of the beam during hardening.

Figure 7 compares strains during concrete hardening. When the sum of strains is positive, the concrete is under tension and fracturing strain is introduced. No plastic strain was found in the calculation, which means no concrete irreversible damage under compression took place. Note that temperature strain has the largest effect at early ages.

12 APPLICATION EXAMPLE

The presented model was applied in a practical engineering problem of cracking in newly built massive concrete columns. The analyzed columns support the boiler-room of a newly built 660MW coal power plant (see Figure 8). Altogether 4 columns with dimensions 5x5x4.57 m support the boiler chamber with total weight of about 672 MN. Approximately 1 year after the construction of the massive columns, vertical cracks up to 0.5 mm were detected in the middle of the columns (see Figure 9) . It was assumed that the hydration heat, shrinkage and insufficient reinforcement (Figure 10) might have been the main reason for this cracking. The presented model was used to confirm this assumption and to evaluate the effect of this initial damage on the strength and reliability of these critical load bearing elements.

Figure 8: Boiler-room building, the analyzed columns are located in the basement.

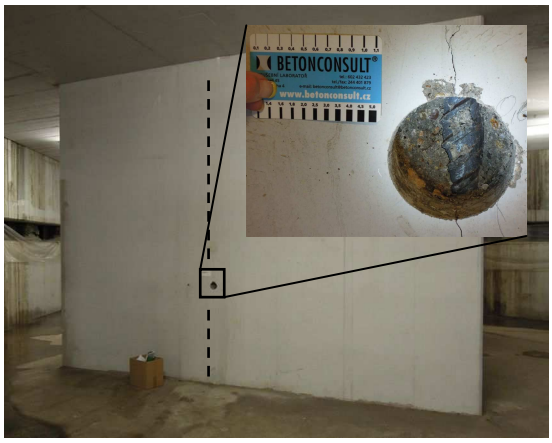

Figure 9: Location of the vertical crack

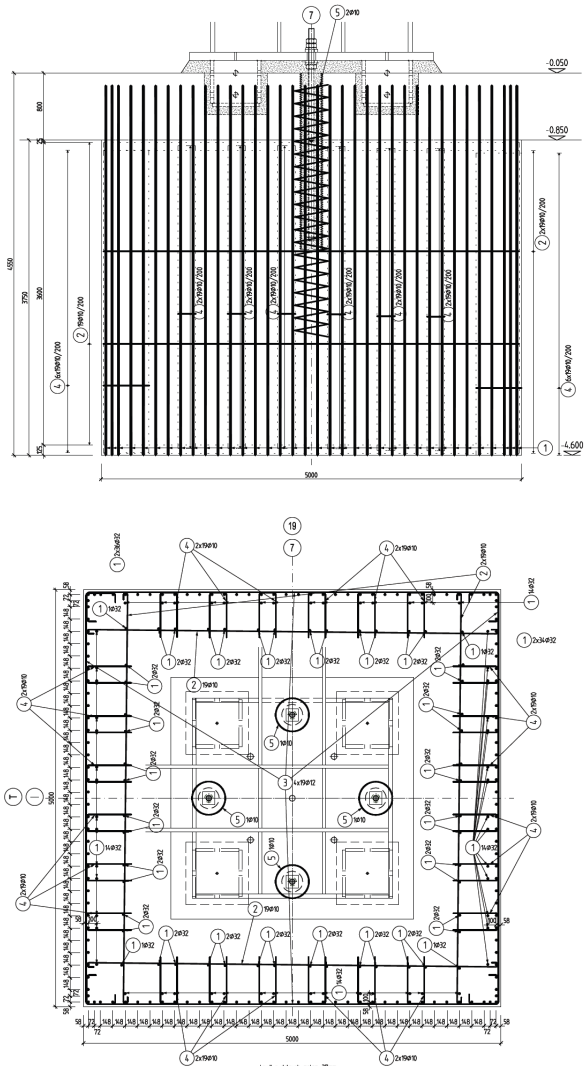

Figure 10: Column reinforcement

The analysis was divided into three phases: the period 3-180 days, i.e. from the column casting up to the gradual introduction of the loads. The second period from 180-720 days, which represents the time of the building construction when the cracks were detected. The crack pattern and crack width at this time is shown in Figure 11. In the third phase, the columns are loaded up to 100% of the design load and overloaded up to failure to evaluate their ultimate strength (Figure 13).

The analysis showed that the cracking was mainly caused by the hydration heat, which reached about 61°C in 8 days after casting (Figure 12). The reinforcement was arranged only near to the column surfaces, and there was no reinforcement spanning from one side to the other, thus there was nothing to resist the temperature strains due to hydration. The predicted crack with is about 0.23 mm, which compares well with the measured crack widths in the range of 0.1-0.5 mm.

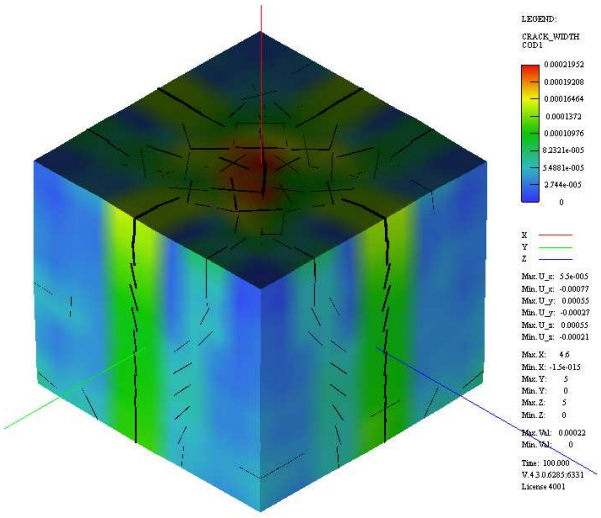

Figure 11: Calculated cracking pattern and crack width of 0.23 mm after 720 days**.**

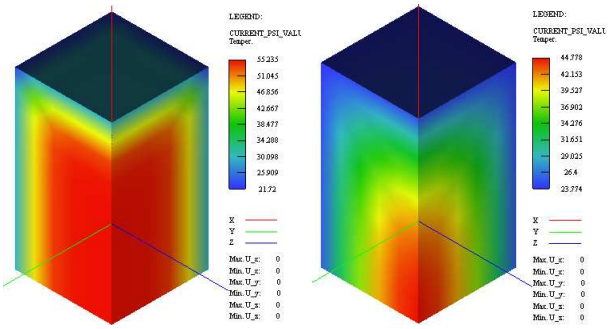

Figure 12: Calculated temperature fields after 8 (left) and 40 (right) days.

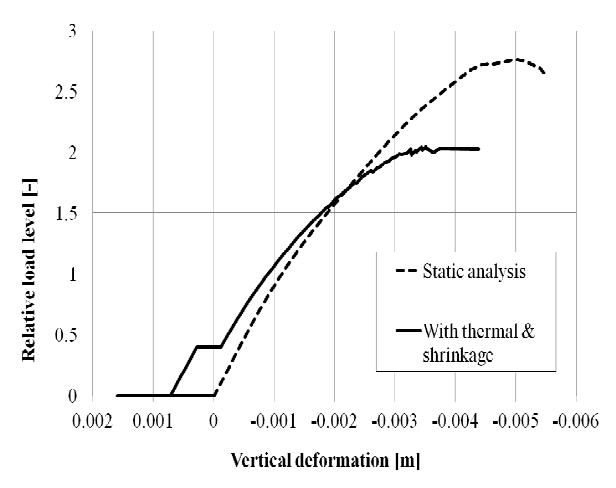

Figure 13: Comparison of load-displacement response for the analysis without (i.e. static) and with temperature and shrinkage effects.

The load carrying capacity of the columns is shown in Figure 13. It compares the load-displacement response of a pure static analysis with the analysis based on the presented hydro-thermo-mechanical model. The result of the new model is depicted by a solid line. Initially, there is no load, but the vertical deformation increases due to the thermal effects, which is followed by a decrease due to shrinkage. After that the load is increased up to 40% of the design load to simulate the situation after 720 days. This load level is kept constant for 540 days while the creep and shrinkage further decreases the deformation. This is represented by the short horizontal line. After that the column is loaded up to failure. This response can be contrasted by the pure static analysis depicted by the dashed line, which shows a smooth response up to failure. The analysis confirmed that the columns have a sufficient load carrying capacity, i.e. about 200% of the design load, but their strength was significantly reduced by almost 30%.

12 CONCLUSIONS

The combined thermo-hydro-mechanical model was presented suitable for modelling the behaviour of young concrete structures. The behaviour of the model was demonstrated on a hydrating concrete beam with experimental results. The developed model was successfully applied to a practical engineering problem. It was possible to quantitatively evaluate the effect of early age cracking on the structural strength and reliability.

The presented model was developed within the project FR-TI1/ 612 from the Ministry of Industry and Trade of the Czech Republic. The presented results were created using software tools developed during the project TA01011019 from Czech Technological Agency.

REFERENCES

[1] V. Cervenka, J. Cervenka, and L. Jendele, "Atena Program Documentation, Part 1-7", Prague: Cervenka Consl.,2000-2012.

[2] M. Nilsson, "Thermal Cracking of Young Concrete. Partial Coefficients, Restraint Effects and Influence of Casting Joints", Thesis, Lulea, Sweden, Lulea Univeristy of Technology, , 2000.

[3] A.M. Neville, "Properties of Concrete": John Wiley & Sons, Inc.,1997.

[4] D. Gawin, F. Pesavento, and B.A. Schrefler, "Hygro-thermo-chemomechanical Modelling of Concrete at Early Ages and Beyond. Part I: Hydration and Hygro-thermal Phenomena", Int. Journal for Numerical Methods in Eng., 67(3), 299-331, 2006.

[5] R. Faria, M. Azenha, and J.A. Figueiras, "Modelling of Concrete at Early Ages: Application to an Externally Restrained Slab", Cement and Concrete Composites, 28(6), 572-578, 2006.

[6] M. Cervera, J. Oliver, and T. Prato, "Thermo-chemo-mechanical Model for Concrete. I: Hydration and Aging", Jour. Eng. Mech. ASCE, 125(9), 1018-1027, 1999.

[7] C. Hellmich, H.A. Mang, and F.J. Ulm, "Hybrid Method for Quantification of Stress States in Shotcrete Tunnel

Shells: Combination of 3D in situ Displacement Measurements and Thermochemoplastic Material Law", Computer and Structures, 79(2103 – 2115), 2001.

[8] L. Jendele, V. Smilauer, and J. Cervenka, "Multi-scale Heat and Moisture Coupled Modeling in Hardening Concrete Structures", Computer and Structures, in review, 2011.

[9] D.P. Bentz, "Transient Plane Source Measurements of the Thermal Properties of Hydrating Cement Pastes", Materials and Structures, 40(10), 1073-1080, 2007.

[10] H.M. Kuenzel, Simultaneous Heat and Moisture Transport in Building Components. 1D and 2D calculation using simple parameters. Fraunhofer Inst. of Building Physics: Stuttgart1995.

[11] Z.P. Bazant, "Mathematical Modeling of Creep and Shrinkage of Concrete", New York: John Wiley & Sons,1988.

[12] Z.P. Bazant, "Prediction of Concrete Creep Effects Using Age-Adjusted Effective Modulus Method", ACI Journal, 69 (4), 212-217, 1972.

[13] L. Jendele and D.V. Phillips, "Finite Element Software for Creep and Shrinkage in Concrete", Computer and Structures, 45 (1), 113-126, 1992.

[14] Z.P. Bazant and S. Baweja, eds. Creep and Shrinkage Predicition Model for Analysis and design of Concrete Structures: Model B3. Creep and Shrinkage of Concrete, ed. A. Al-Manaseer, ACI Special Publicatino, 1999.

[15] J. Cervenka, V. K. Papanikolaou, Three Dimensional Combined Fracture-Plastic Material Model for Concrete, International Journal of Plasticity, 24(12), pp. 2192-2220

[16] R. De Borst, "Non-linear analysis of frictional materials", Thesis, Delft, Delft University of Technology, 1986.

[17] Z.P. Bazant and B.H. Oh, "Crack Band Theory for Fracture of Concrete", Material and Structures, 16, 155-177, 1983.

[18] D.D. Hordijk, "Local Approach to Fatigue of Concrete", Thesis, Delpht, Delft University of Technology, 1991.

[19] P. Menetrey and K.J. Willam, "Triaxial Failure Criterion for Concrete and its Generalization", ACI Structural Journal, 92(3), 311-318, 1995.